RSC Advances

PAPER

View Article Online
View Journal | View Issue

Cite this: *RSC Adv.*, 2024, **14**, 39268

Calcium-atom-modified boron phosphide (BP) biphenylene as an efficient hydrogen storage material†

Yusuf Zuntu Abdullahi, [ab] Ikram Djebablia, *[cd] Tiem Leong Yoon [e] and Lim Thong Leng[f]

Porous nanosheets have attracted significant attention as viable options for energy storage materials because of their exceptionally large specific surface areas. A recent study (*Int. J. Hydrogen Energy*, 2024, **66**, 33–39) has demonstrated that Li/Na-metalized inorganic BP-biphenylene (b-B_3P_3) and graphenylene (g-B_6P_6) analogues possess suitable functionalities for hydrogen (H_2) storage. Herein, we evaluate the H_2 storage performance of alkaline earth metal (AEM = Be, Mg, Ca)-decorated b-B_3P_3 and g-B_6P_6 structures based on first-principles density functional theory (DFT) calculations. Our investigations revealed that individual Be and Mg atoms are not stable on pure b-B_3P_3 and g-B_6P_6 sheets, and the formation of aggregates is favored due to their low binding energy to these surfaces. However, the binding energy improves for Ca-decorated b-B_3P_3 (b-B_3P_3(*m*Ca)) and g-B_6P_6 (g-B_6P_6(*n*Ca)) structures, forming stable and uniform *m*Ca(*n*Ca) (*m* and *n* stand for the numbers of Ca atom) coverages on both sides. Under maximum hydrogenation, the b-B_3P_3(8Ca) and g-B_6P_6(16Ca) structures exhibited the ability to adsorb up to 32H_2 and 48H_2 molecules with average adsorption energy (E_a) values of −0.23 eV per H_2 and −0.25 eV per H_2, respectively. Gravimetric H_2 uptakes of 7.28 wt% and 5.56 wt% were found for b-B_3P_3(8Ca)@32H_2 and g-B_6P_6(16Ca)@48H_2 systems, exceeding the target of 5.50 wt% set by the US Department of Energy (DOE) to be reached by 2025. Our findings indicate the importance of these b-B_3P_3 and g-B_6P_6 sheets for H_2 storage technologies.

Received 10th October 2024
Accepted 22nd November 2024

DOI: 10.1039/d4ra07271e

rsc.li/rsc-advances

1 Introduction

Growing concerns over environmental pollution and the limited supply of fossil fuels have driven the pursuit of clean energy sources.[1,2] Hydrogen (H_2) is regarded as a sustainable and alternative energy source capable of eradicating the use of fossil fuels, especially in transportation applications.[3–5] However, one of the main hindrances to the advancement of H_2 technology is creating small, light, safe, and affordable storage systems with large storage capacity under practical conditions.[3,6] Solid-state H_2 storage materials, which store H_2 *via* the physisorption or chemisorption method, have been extensively investigated as a promising approach to overcome the challenges associated with gas or liquid H_2 storage, which requires very high pressure (350–700 bar).[3,7,8] According to the US Department of Energy (DOE), by 2025 an ideal H_2 storage material should attain gravimetric and volumetric capacity greater than 5.5 wt% and 30 g L^{-1}, with adsorption energy (E_a) between 0.2 and 0.6 eV per H_2.[9–11] By meeting these minimum thresholds, an adsorbent material will allow suitable reversible H_2 storage under ambient conditions.

To date, a wide range of materials, including carbon-based materials,[12–14] MXenes,[15,16] metal–organic-frameworks (MOFs)[17–19] covalent organic frameworks (COFs)[20–22] and related low-dimensional materials[23–32] have attracted a significant number of studies in several research areas, including spintronics, batteries, optoelectronics and catalysis. Porous two-dimensional (2D) materials, in particular organic/inorganic-based biphenylene (BPN) or graphenylene (BPC) sheets, are ideally suited for H_2 storage applications.[33–44] However, the weak interaction between these surfaces and H_2 molecules (due to low E_a values) reduces their H_2 storage capacities. Extensive theoretical studies have shown that the

[a]*Department of Physics, Aydin Adnan Menderes University, Aydin 09010, Turkey*
[b]*Department of Physics, Faculty of Science, Kaduna State University, P.M.B. 2339, Kaduna State, Nigeria*
[c]*Radiation and Matter Physics Laboratory, Matter Sciences Department, Mohamed-Cherif Messaadia University, P.O. Box 1553, Souk-Ahras, 41000, Algeria. E-mail: ik.djebablia@univ-soukahras.dz*
[d]*Physics Laboratory at Guelma, Faculty of Mathematics, Computing and Material Sciences, University 8 May 1945 Guelma, P.O. Box 401, Guelma 24000, Algeria*
[e]*School of Physics, Universiti Sains Malaysia, 11800 Penang, Malaysia*
[f]*Faculty of Engineering and Technology, Multimedia University, Jalan Ayer Keroh Lama, 75450 Melaka, Malaysia*

† Electronic supplementary information (ESI) available: Snapshots of the molecular dynamics simulations, Electron Localization Function (ELF) and total density of states for optimized structures of b-B_3P_3(8Ca)@32H_2 and g-B_3P_3(8Ca)@48H_2 structures. See DOI: https://doi.org/10.1039/d4ra07271e

metal-atom decoration technique[45–47] can be effective for improving the E_a, resulting in higher H_2 uptake. For instance, Denis *et al.*[33] studied the H_2 storage performance of BPN with adsorbed Li-adatoms, and obtained a H_2 uptake of 7.4 wt%, with an averaged E_a of 0.20 eV per H_2. In addition, ultrahigh H_2 storage capacity values of 11.9 wt% and 11.63% for K- and Ca-decorated BPN structures was predicted by Mahamiya *et al.*[34] Singh *et al.*[48] have found 11.07 wt% H_2 uptake near ambient temperature for a Sc-decorated BPN structure. Kaewmaraya *et al.*[35] reported 6.66 wt% and 6.76 wt% H_2 storage capacities for Li/Na-decorated divacancy BPN. Moreover, H_2 storage analysis was carried out on Li-decorated BPN and Li-decorated N-doped BPN by Zhang *et al.*[38] They reported H_2 uptakes of 9.581 wt% and 10.588 wt% for Li-decorated BPN and Li-decorated N-doped BPN, respectively. In another separate study, adsorption of H_2 on a Li-decorated B-doped BPN structure has been explored by Ma *et al.*[40] Their analysis indicated that the H_2 storage capacity value changed from 6.30 wt% to 19.22 wt% as a function of Li-ion concentration, which increased from 7.69% to 25.00%. On the other hand, Hussain *et al.*[36] used light metals to enhance the H_2 storage capacity value of BPC sheets. Their results revealed that the BPC can accommodate 20 H_2 molecules with storage capacity values between 4.90 wt% and 6.14 wt% under operating conditions. Additionally, Boezar *et al.*[49] evaluated the H_2 adsorption behavior of transition metal (Fe, Sc and Ti) decorated BPC structures. Their studies indicate that these structures can take up to 20 H_2 molecules with average E_a values higher than 0.2 eV per H_2. Structures with Li(Na)-atom-decorated inorganic graphenylene (IGP) based on SiC (Li(Na)@IGP-SiC) have been investigated by Martins *et al.*[37] for H_2 storage performance. Their calculations revealed that Li(Na)@IGP-SiC can take up to 48 H_2 molecules, yielding an enhanced H_2 storage capacity value of 8.27 wt% (6.78 wt%) for Li(Na)@IGP-SiC structures. Following this use of IGP sheets, Djebablia *et al.*[39] recently studied the H_2 performance of b-BP(Li, Na, K)/g-BP(Li, Na, K) structures. They found that each adatom binds strongly on the host b-BP/g-BP surfaces and adsorbs multiple H_2 molecules, resulting in uptakes of 9.05% and 6.99% for b-BP(Li) and g-BP(Li) structures, respectively, under practical conditions.

Motivated by the results mentioned above, we investigate the effect of alkaline earth metal (AEM = Be, Mg, Ca)-decorated b-B_3P_3 and g-B_6P_6 sheets for H_2 storage applications, using spin-polarized density functional theory (DFT). The obtained results reveal that Be and Mg atoms bind weakly to the b-B_3P_3 and g-B_6P_6 sheets. In contrast, Ca atoms exhibit a strong binding energy, making them suitable hosts for adsorbing a considerable number of H_2 molecules. Meanwhile, addition of H_2 molecules on the Ca-decorated b-B_3P_3 (b-B_3P_3(Ca)) and g-B_6P_6 (g-B_6P_6(Ca)) structures was analyzed to fully understand their H_2 storage performance. Moreover, the b-B_3P_3(Ca) and g-B_6P_6(Ca) structures reached storage capacities of 7.28 wt% and 5.56 wt%, respectively, exceeding the target of 5.50 wt% set by the US DOE to be attained by 2025. For the sake of convenience, b-B_3P_3(Ca) and g-B_6P_6(Ca) with adsorbed $p(q)H_2$ molecules are named b-B_3P_3(mCa)@pH_2 and g-B_6P_6(nCa)@qH_2, respectively (p/q and n/m correspond to the numbers of adsorbed H_2 molecules and Ca adatoms, respectively).

2 Computational details

The spin-polarized DFT[50] calculations on the ground-state properties of all studied structures have been implemented in the Vienna *ab initio* simulation package (VASP).[51] The projector augmented-wave (PAW) approach[52] was used to describe ion–electron interactions. The exchange–correlation functional was treated using the generalized gradient approximation (GGA) of the Perdew–Burke–Ernzerhof (PBE) functional.[52] The van der Waals (vdW) interaction correction was added through the DFT-D2 approach.[53] It should be noted that the PBE-D2 vdW correction is prone to overestimating adsorption energy values in certain cases, which could have an impact on the conclusions drawn.[54] During the structural optimization calculations, the Brillouin zone (BZ) of all studied structures was sampled using the Monkhorst–Pack approach[55] with (6 × 6 × 1) and (12 × 12 × 1) grids for self-consistency and total density-of-state computations, respectively. We used a plane-wave basis set with a kinetic energy cut-off of 500 eV to expand the wave functions. We set a vacuum layer at least 18 Å thick perpendicularly to the cell dimension for all calculations. The convergence criteria for energy and force for all calculations were set at 0.001 eV $Å^{-1}$ and 10^{-5} eV, respectively. To assess the thermal stability of all studied b-B_3P_3(Ca) and g-B_6P_6(Ca) structures, *ab initio* molecular dynamics (AIMD) simulations have been performed at room temperature (300 K).[56] In the *NVT* ensemble, 1 fs for 5000 iterations and the Nosé thermostat were used for the MD simulation parameters. Bader analysis[57] was employed to study the charge transfer mechanism. With the aid of VESTA software,[58] the charge distribution and structural analysis were obtained.

Considering the b-B_3P_3(Ca) case, the average adsorption energy (E_a) is defined as:

$$E_a = (E_{\text{b-}B_3P_3(m\text{Ca})} - E_{\text{b-}B_3P_3} - mE_{\text{Ca}})/m \quad (1)$$

where $E_{\text{b-}B_3P_3(m\text{Ca})}$, $E_{\text{b-}B_3P_3}$ and E_{Ca} denote the total energy of b-B_3P_3 decorated with mCa adatoms, the pure b-B_3P_3 sheet and isolated Ca adatoms, respectively. We used the same E_a procedure for the g-B_6P_6(Ca) case.

The average E_a for the b-B_3P_3(mCa)@pH_2 structure is computed as:

$$E_a = (E_{\text{b-}B_3P_3(8\text{Ca})@pH_2)} - E_{\text{b-}B_3P_3(8\text{Ca})} - pE_{H_2})/p \quad (2)$$

where the $E_{\text{b-}B_3P_3(8\text{Ca})@pH_2)}$ and E_{H_2} terms denote the total energy of the b-B_3P_3(8Ca)@pH_2) structure and isolated H_2 molecules, respectively. We used the same E_a procedure for the g-B_6P_6(nCa)@qH_2 case.

The H_2 molecule storage capacity (wt%) has been evaluated by employing the following expression:

$$H_2(\text{wt}\%) = \frac{mH_2}{(mH_2 + m_{\text{b-}B_3P_3(8\text{Ca})(\text{b-}B_3P_3(8\text{Ca}))})} \times 100 \quad (3)$$

Here, mH_2 and $m_{b\text{-}B_3P_3(8Ca)(b\text{-}B_3P_3(8Ca))}$ stand for the mass of H_2 uptake and the mass of the b-B_3P_3(8Ca)(b-B_3P_3(8Ca)) structure, respectively.

The average desorption temperature (T_d) of the b-B_3P_3(8Ca)@pH_2 and g-B_6P_6(16Ca)@qH_2 systems has been estimated by employing the van't Hoff equation,[59] expressed as:

$$T_d = \frac{E_a}{k_B}\left(\frac{\Delta S}{R} - \ln P\right)^{-1} \quad (4)$$

where E_a is the averaged E_a (J per H_2) of H_2 molecules adsorbed on the b-B_3P_3(8Ca) and g-B_6P_6(16Ca) systems. The entropy change (ΔS), the Boltzmann constant (k_B), the universal gas constant (R) and the atmospheric pressure (P) are taken as 75.44 J K^{-1} mol^{-1}, 1.380 × 10^{23} J K^{-1}, 8.62 × 10^{-5} eV K^{-1} and 1 atm, respectively.

3 Results and discussion

3.1 Adsorbent structures

This paper expands on the recently reported H_2 storage on b-B_3P_3(Li) and g-B_6P_6(Li) structures,[39] by investigating the H_2 storage performance of b-B_3P_3(Mg, Be, Ca) and g-B_6P_6(Mg, Be, Ca) structures. To begin with, we construct b-B_3P_3 and g-B_6P_6 supercells in (2 × 2 × 1) dimensions, as depicted in Fig. 1. Each (2 × 2 × 1) b-B_3P_3/g-B_6P_6 sheet consists of 24 B, 24 P, and 4 Ca atoms. Henceforth, we shall consider the (2 × 2 × 1) supercell of b-B_3P_3/g-B_6P_6 as b-$B_{12}P_{12}X_4$/g-$B_{24}P_{24}X_4$ sheets. The optimized lattice constants were evaluated to be $a = 11.80$ Å and $b = 9.75$ Å, and $a = b = 17.61$ Å, respectively, for b-B_3P_3 and g-B_6P_6 sheets, in good agreement with a recently reported paper.[60] It is well-known that pure 2D materials[24,33–36,39,61–63] form weak interactions with H_2 molecules, which reduces their storage capacities. However, metalization of these b-B_3P_3 and g-B_6P_6 sheets with AEM (Be, Mg, Ca) adatoms is an efficient route to improve the H_2 chemical activity on their surfaces. We have examined eight distinct adsorption sites on the b-B_3P_3 and g-B_6P_6 sheets to determine the preferred location of single AEM atoms. Fig. 1 illustrates these adsorption sites, which are at the top of the boron (T_B) and phosphorus (T_P) atoms, the octagonal/decagonal cavity (A_1), the square (A_2) and hexagonal (A_3) rings, and the bridging sites (A_4, A_5 and A_6).

To achieve a uniform distribution, each AEM adatom must bind firmly to these b-B_3P_3 and g-B_6P_6 sheets. A negative E_a value signifies a stable configuration. Conversely, a positive E_a value suggests an unfavorable adsorption process. The calculated E_a values of single AEM adatoms at the most stable b-B_3P_3 and g-B_6P_6 sites are presented in Fig. 2. We have found that the Be and Mg adatoms bind on the b-B_3P_3 and g-B_6P_6 sheets with very small E_a values. Additionally, their cohesive energy (E_c) is notably greater than their E_a values on the these surfaces. Hence, these metals would rather form clusters than bind separately to the b-B_3P_3 and g-B_6P_6 sheets. Therefore, we have not considered b-B_3P_3(Be), b-B_3P_3(Mg), g-B_6P_6(Be) and g-B_6P_6(Mg) structures for the H_2 adsorption calculations (see Fig. 2). However, the E_a values of Ca-decorated b-B_3P_3 and g-B_6P_6 sheets are found to be −2.82 eV and −2.62 eV, respectively, larger than the E_c value of the bulk Ca atom (1.84 eV).[64] Bader charge (Q) analysis[57] confirms that there was a significant transfer of 1.40 e^- from the Ca^+ ion to the b-B_3P_3/g-B_6P_6

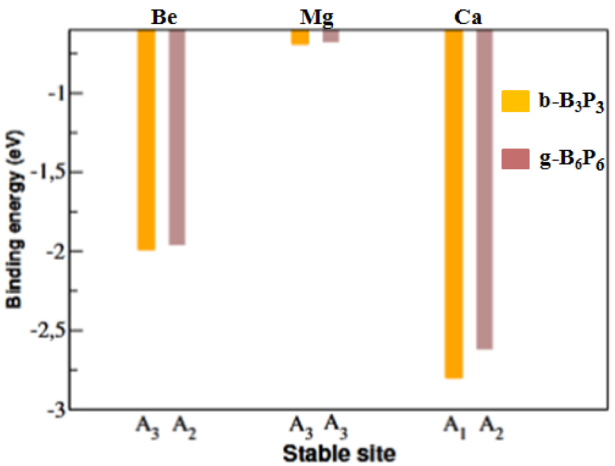

Fig. 2 The E_a values of b-B_3P_3(Be, Mg, Ca) and g-B_6P_6(Be, Mg, Ca) structures.

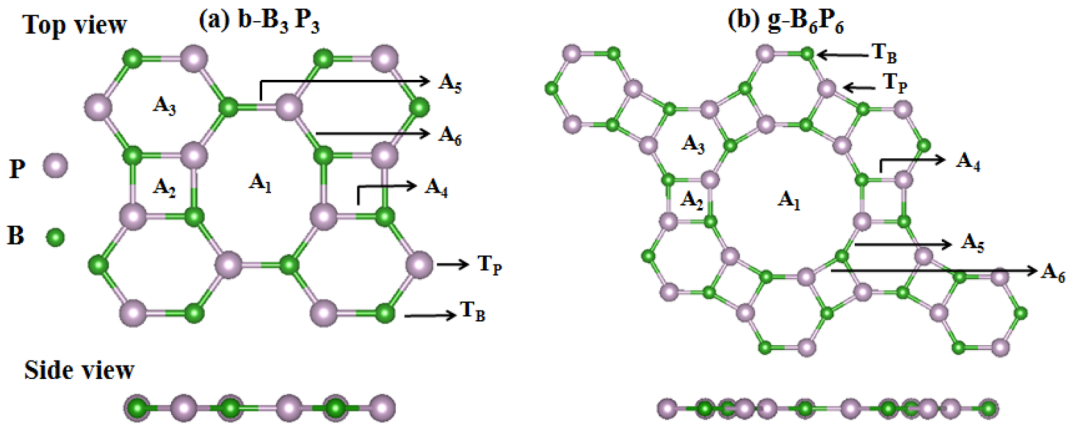

Fig. 1 Geometric structures of (a) b-B_3P_3 and (b) g-B_6P_6 sheets: top and side views with illustration of the available binding sites (A_1, A_2, A_3, A_4, A_5, A_6, T_B and T_P).

monolayer, as compared with 1.32/1.02 e^- from Be^+/Mg^+ ions, respectively. This shows a favorable ionic bonding between Ca adatoms and the b-B_3P_3/g-B_6P_6 surfaces. The obtained E_a values correlate with the estimated electron transfer values. Hence, these stable b-B_3P_3(Ca) and g-B_6P_6(Ca) structures are considered for further studies. Because they have a large surface area, the b-B_3P_3 and g-B_6P_6 sheets are expected to possess the ability of binding multiple Ca adatoms. This could significantly improve their H_2 storage performance. Consequently, we introduced several Ca adatoms to investigate their binding properties. Our findings revealed that eight Ca adatoms can be adsorbed on the b-B_3P_3 sheet, with an E_a value of −2.46 eV per Ca. The g-B_6P_6 sheet can take up to 16Ca adatoms with E_a values of −2.47 eV per Ca. We have also carried out another analysis to illustrate the stability of dispersed Ca adatoms on b-B_3P_3 and g-B_6P_6 surfaces compared to Ca dimer formation or aggregation into clusters. This is done by comparing the single Ca atom and dimer E_a values for adsorption on these surfaces. As we know, if the Ca dimer binding on the surface becomes less stable compared to single-atom binding, cluster formation can be avoided. Hence, the clustering energy ($E_{cluster}$) was determined by comparing the E_a of the dimer to that of the single Ca adsorbed on the b-B_3P_3/g-B_6P_6 surfaces. If the $E_{cluster}$ has a positive (negative) value, it means that the Ca atoms are susceptible to cluster formation (dispersion). The obtained $E_{cluster}$ values are −0.23 and −0.79 eV for b-B_3P_3 and g-B_6P_6 monolayers, respectively. Clearly, all Ca atoms possess negative clustering energy values on these b-B_3P_3 and g-B_6P_6 surfaces. It can be inferred that the Ca atoms that are dispersed on the b/g-BP surfaces are generally stable and Ca cluster formation can be avoided. Additionally, Fig. S4 in the ESI File† confirms the dynamic stability of these b-B_3P_3 and g-B_6P_6 structures with adsorbed Ca adatoms.

Table 1 lists the calculated E_a values, the average heights of Ca adatoms from the b-B_3P_3(g-B_6P_6) sheets (bond lengths, $d_{Ca-b\text{-}B_3P_3(g\text{-}B_6P_6)}$) and the amounts of charge released by the Ca adatoms. The top and side views of the optimized b-B_3P_3(8Ca) and g-B_6P_6(16Ca) geometries are shown in Fig. S1.† For the b-B_3P_3(8Ca) and g-B_6P_6(16Ca) structures, there was an absence of any indication of structural reconstruction after optimization. Additionally, there is no tendency for Ca adatoms to cluster on the b-B_3P_3 and g-B_6P_6 surfaces.

Table 1 We provide the adsorption energies (E_a in eV per Ca), bond lengths ($d_{Ca-b\text{-}B_3P_3(g\text{-}B_6P_6)}$) and amounts of charge transfer (Q) (from Ca to b-B_3P_3 and g-B_6P_6 sheets) for the b-B_3P_3(mCa) and g-B_6P_6(nCa) structures. The $d_{Ca-b\text{-}B_3P_3(g\text{-}B_6P_6)}$ is the averaged bond length along the z-axis between Ca adatoms and all the B/P atoms in the b-B_3P_3 and g-B_6P_6 structures. m/n represents the number of Ca adatoms

System	m/n	E_a	$d_{Ca-b\text{-}B_3P3(g\text{-}B6P6)}$ (Å)	Q (e^-)
b-B_3P_3(mCa)	1	−2.80	1.23	1.39
	4	−2.31	1.54	1.31
	8	−2.46	1.81	1.11
g-B_6P_6(nCa)	1	−2.62	1.79	1.39
	8	−2.35	2.28	1.15
	16	−2.47	1.98	1.09

We provide charge analysis calculations for the b-B_3P_3(mCa) and g-B_6P_6(nCa) structures to illustrate the charge transferred from the Ca adatoms to the b-B_3P_3(g-B_6P_6) sheets (see Table 1). There is a significant charge transfer from Ca^+ ions to the b-B_3P_3 and g-B_6P_6 sheets for all structures. As a result, Ca adatoms and these surfaces form an ionic bond, as confirm by the ELF plots in Fig. S3.† It should be noted that the obtained E_a values agree with the obtained electron transfer values. The averaged bond length along the z-axis between Ca adatoms and all the B/P atoms in the b-B_3P_3 and g-B_6P_6 surfaces corresponds well with the E_a values listed in Table 1. It shows that the stronger the interaction, the lower the bond length, which affects the values of E_a. Also, the thermal stability of the b-B_3P_3(Ca) and g-B_6P_6(Ca)) structures was evaluated through AIMD at 300 K for a duration of 5 ps. In Fig. S4,† we have shown the oscillation range of total energy against time step at 300 K. According to the figure, the energy oscillations for each atom fluctuate within a fixed range on the order of meV. In addition, in Fig. S4† we give images of the side and top views of the b-B_3P_3(Ca) and g-B_6P_6(Ca)) structures. It is clear that these structures maintain their structural integrity at room temperature without any visible structural reconstructions. It is evident that these b-B_3P_3(Ca) and g-B_6P_6(Ca)) structures are suitable ones for H_2 storage applications under ambient conditions.

3.2 H_2 adsorption on b-B_3P_3(8Ca) and g-B_6P_6(16Ca) structures

Firstly, the H_2 molecule is introduced at a given height above the stable adsorption site of the b-B_3P_3(8Ca) and g-B_6P_6(16Ca) structures. Then, the b-B_3P_3(Ca)@H_2 and g-B_6P_6(Ca)@H_2 systems are fully relaxed without any geometry restriction. Subsequently, a number of H_2 molecules was incrementally added until the maximum adsorption limit was reached. According to the E_a values obtained for b-B_3P_3(8Ca) and g-B_6P_6(16Ca), there is strong physisorption and chemisorption of H_2 molecules. These structures provide a better binding of H_2 molecules than those obtained from the pristine b-B_3P_3@H_2 and g-B_6P_6@H_2 systems.[39] Fig. 4 displays all the remaining estimated E_a values. It is revealed that the b-B_3P_3(8Ca) structure can adsorb up to 32 H_2 molecules, with an average E_a value of −0.23 eV per H_2. On the other hand, the g-B_6P_6(16Ca) structure can retain 48H_2 molecules with an average E_a value of −0.25 eV per H_2. It should be noted that these estimated E_a values show the tendency to accommodate more H_2 molecules on the b-B_3P_3(8Ca) and g-B_6P_6(16Ca) structures. In comparison with the earlier results based on DFT calculations, our estimated moderate H_2 E_a values are better than or comparable with those reported for metallized boron monoxide, boron hydride and Me–C_8B_5 monolayers.[47,65,66] The significantly negative E_a value means a stronger interaction of H_2 molecules on b-B_3P_3(8Ca) and g-B_6P_6(16Ca) structures. The E_a value we obtained for the maximum of adsorbed H_2 molecules is within the above-mentioned acceptable range required for a H_2 storage material. This means that the H_2 molecule has been strongly physisorbed onto these b-B_3P_3(8Ca) and g-B_6P_6(16Ca) structures. Fig. 3 shows the relaxed structures of the b-B_3P_3(8Ca)@32H_2

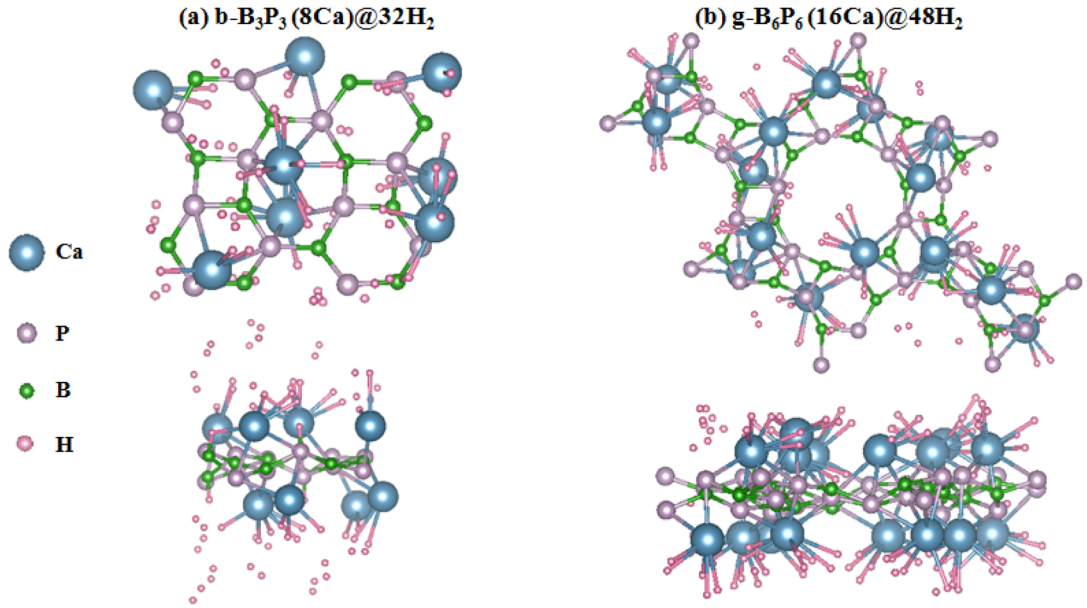

Fig. 3 The optimized structures with maximum adsorbed H_2 molecules: (a) b-B_3P_3(8Ca) and (b) g-B_6P_6(16Ca) structures.

and g-B_6P_6(16Ca)@48H_2 structures, whereas the remaining b-B_3P_3(8Ca)@pH_2 and g-B_6P_6(16Ca)@qH_2 structures are illustrated in Fig. S5 and S6.† We also provide, in Table 2, the numbers (p,q) of H_2 molecules adsorbed on the b-B_3P_3(8Ca) and g-B_6P_6(16Ca) structures, the E_a (eV per H_2), the average H–H bond length (d_{H-H}) and the corresponding H_2 capacity (wt%).

It well-known that the interaction of an adsorbent surface with a H_2 molecule can be attributed to the electronic properties of the host material and the vdW forces between the H_2 and the surface. For weak vdW forces, the H_2 molecule can be physisorbed on the surface. Conversely, the H_2 molecule may dissociate into double H atoms and form a strong chemical bond with the surface atoms *via* a chemisorption mechanism, as previously reported.[47,63,67] It is noted from the optimized structures that 4 H_2 and 12 H_2 molecules are adsorbed through a physisorption process on the b-B_3P_3(8Ca) structure. However, we found that for adsorption of 8 H_2 and 16 H_2 molecules, one H_2 molecule is dissociated into 2H atoms, and four 4 H_2 molecules show a tendency to dissociate into 8 H atoms. In these cases, we found that the average H–H bond length is extended from 0.74 Å (gas-phase H–H distance) to 0.87 and 0.97 Å, showing that the adsorption of H_2 molecules on the b-B_3P_3(8Ca) structure arises through a strong physisorption process (see Fig. 4).

Table 2 Number of H_2 molecules, adsorption energies E_a (eV per H_2), the corresponding average bond lengths for H_2 molecules d(H–H), H_2 storage capacity W (wt%), and desorption temperature T_D (K) for the b-B_3P_3(8Ca) and g-B_6P_6(16Ca) structures

System	Number of H_2	E_a (eV per H_2)	d(H–H)	T_D (K)	W (wt%)
b-B_3P_3(8Ca)	1	−0.38	0.762	486.21	0.24
	4	−0.16	0.763	204.72	0.97
	8	−0.35	0.970	447.82	1.92
	12	−0.19	0.762	243.10	2.86
	16	−0.20	0.869	255.90	3.78
	32	−0.23	0.973	294.28	7.28
g-B_6P_6(16Ca)	1	−1.35	0.769	1727.32	0.12
	8	−0.34	0.770	435.03	0.97
	16	−0.51	1.081	652.54	1.92
	24	−0.35	0.947	447.82	2.86
	48	−0.25	0.840	319.87	5.56

On the other hand, for the g-B_6P_6(16Ca) structure, the adsorption of 8 H_2 molecules occurs through physisorption (molecular form). However, 3 H_2 molecules are dissociated into 6 H atoms in the case of 16 adsorbed H_2 molecules, while 2 H_2 molecules are dissociated into 4 H atoms in the cases of adsorption of 24 H_2 and 48 H_2 molecules. Their corresponding H–H bond lengths range between 0.84–1.08 Å. The tendency towards dissociation is attributed to the larger E_a values, which lead to an expanded d_{H-H} value for H_2 molecules (see Fig. 4). According to eqn (3), the estimated H_2 storage capacities are 7.28% and 5.56% for the b-B_3P_3(8Ca) and g-B_6P_6(16Ca) structures, respectively, exceeding the US DOE requirements. Within the limit of the theoretical method used in the current study, these obtained values are either similar to or higher than those of previously investigated metal-decorated 2D materials,[36,68,69] including the recently reported metallized boron monoxide, boron hydride and Me–C8B5 monolayers.[47,65,66] According to the PDOS plots, all the b-B_3P_3(8Ca)@32H_2 and g-B_6P_6(16Ca)@48H_2 structures exhibit metallic properties (see Fig. S4†). All the structures show evidence of asymmetric spin states around the Fermi level and beyond, which implies the existence of magnetic moments. The states are mainly from the p orbital of the Ca atom, while the s orbital of the H atom makes a small contribution in the vicinity of the Fermi level. Furthermore, there is a relative overlap between the Ca p orbital and the B p and P p orbitals beyond the Fermi level, except for H atoms.

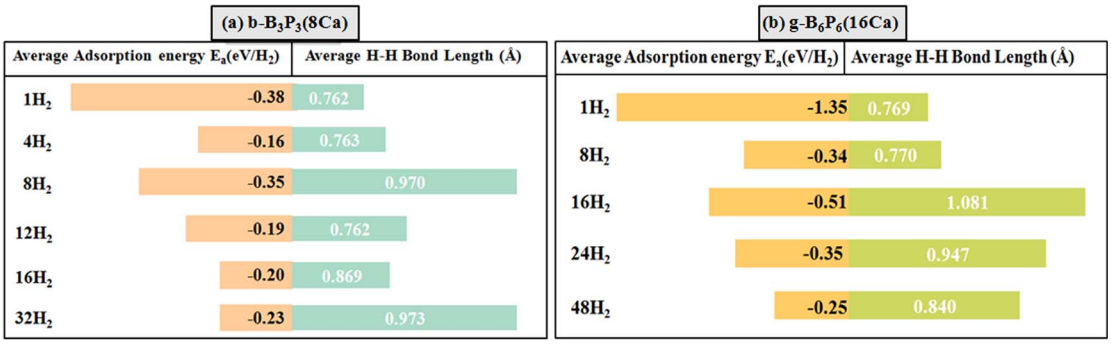

Fig. 4 The average E_a values (eV per H_2) and average bond lengths (H–H) of H_2 molecules for (a) b-B_3P_3(8Ca) and (b) g-B_6P_6(16Ca). The lengths of the bars correspond to the E_a values.

This emphasizes the nature of Ca's interactions with the surroundings, specifically the s orbital of the H atom.

To achieve practical H_2 storage on these b-B_3P_3(8Ca) and g-B_6P_6(16Ca) surfaces, it is necessary to determine the average desorption temperature (T_D). Using eqn (4), the obtained T_D values for the b-B_3P_3(8Ca)@pH_2 and g-B_6P_6(16Ca)@qH_2 structures are summarised in Table 2. The obtained T_D values for the b-B_3P_3(8Ca)@pH_2 and g-B_6P_6(16Ca)@qH_2 structures are found to be in the range of 204–486 K and 319–1727 K, respectively. The T_D values decrease as the number of H_2 molecules increases, while the E_a value decreases. The T_D values for 32 H_2 and 48 H_2 molecules adsorbed on the b-B_3P_3(8Ca) and g-B_6P_6(16Ca) structures are estimated as 294 K and 319 K, respectively. The T_D value is over 9 times larger than the critical point of hydrogen (33 K). The obtained results clearly illustrate the correlation between bond lengths, E_a values, and T_D values. Table 2 reveals the T_D values that correspond to the average lengths of the H–H bonds. The higher T_D values suggest that some molecules are adsorbed through strong physisorption, and the greater H–H bond lengths may lead to dissociation at room temperature. It is worth mentioning that magnetic properties have been proven to be an effective way to regulate H_2's desorption temperature.[70] It is expected that these studied b-B_3P_3(8Ca) and g-B_6P_6(16Ca) structures will enable the storage of H_2 under suitable conditions and have good reversibility.

4 Conclusions

In brief, spin-polarized DFT calculations are employed to investigate the performance of b-B_3P_3 and g-B_6P_6 sheets with adsorbed AEM (Be, Mg, Ca) adatoms for hydrogen storage. We find that Be and Mg adatoms are prone to cluster formation on b-B_3P_3 and g-B_6P_6 surfaces due to their low E_a values. However, the high E_a values for b-B_3P_3(Ca) and g-B_6P_6(Ca) structures show that the Ca adatom is stable and can prevent the segregation of Ca on the b-B_3P_3 and g-B_6P_6 surfaces, even at high concentrations. In addition, It has been demonstrated that the b-B_3P_3(Ca) and g-B_6P_6(Ca) structures are thermally stable at 300 K. Bader charge analysis reveals that Ca transfers an average of 1.11 (1.09) electrons to the b-B_3P_3(Ca) (g-B_6P_6(Ca)) sheets, making the b-B_3P_3(Ca) (g-B_6P_6(Ca)) surfaces suitable for enhanced H_2 molecule storage. In particular, the b-B_3P_3(8Ca) structure can store up to 32 H_2 molecules with an average E_a value of −0.23 eV per H_2. Meanwhile, the g-B_6P_6(16Ca) structure can take up 48 H_2 molecules with an average E_a value of −0.25 eV per H_2. The H_2 molecule storage capacities of the b-B_3P_3(8Ca)@32H_2 and g-B_6P_6(16Ca)@48H_2 structures are 7.28 wt% and 5.56 wt%, respectively. The calculated wt% values are higher than the 5.50 wt% target that needs to be reached by 2025. According to these findings, the b-B_3P_3(8Ca) and g-B_6P_6(16Ca) structures possess the potential to be reversible hydrogen storage media.

Data availability

Data will be made available on request.

Author contributions

Yusuf Zuntu Abdullahi: conceptualization, formal analysis, investigation, software, validation, writing – reviewing and editing, supervision, project administration. Ikram Djebablia: formal analysis, investigation, visualization, validation, writing – reviewing and editing. Tiem Leong Yoon: data curation, formal analysis, writing – reviewing. Lim Thong Leng: data curation, formal analysis, writing – reviewing.

Conflicts of interest

There are no conflicts to declare.

Acknowledgements

The calculations were performed at TUBITAK ULAKBIM, High Performance and Grid Computing Center (TR-Grid e-Infrastructure).

Notes and references

1 M. S. Dresselhaus and I. Thomas, *Nature*, 2001, **414**, 332–337.
2 S. Chu and A. Majumdar, *Nature*, 2012, **488**, 294–303.
3 L. Schlapbach and A. Züttel, *Nature*, 2001, **414**, 353–358.
4 G. W. Crabtree, M. S. Dresselhaus and M. V. Buchanan, *Phys. Today*, 2004, **57**, 39–44.

5 C.-J. Winter and J. Nitsch, *Hydrogen as An Energy Carrier: Technologies, Systems, Economy*, Springer Science & Business Media, 2012.
6 A. W. van den Berg and C. O. Areán, *Chem. Commun.*, 2008, 668–681.
7 P. Jena, *J. Phys. Chem. Lett.*, 2011, **2**, 206–211.
8 C. Tarhan and M. A. Çil, *J. Energy Storage*, 2021, **40**, 102676.
9 S. K. Bhatia and A. L. Myers, *Langmuir*, 2006, **22**, 1688–1700.
10 Y.-H. Kim, Y. Zhao, A. Williamson, M. J. Heben and S. Zhang, *Phys. Rev. Lett.*, 2006, **96**, 016102.
11 R. C. Lochan and M. Head-Gordon, *Phys. Chem. Chem. Phys.*, 2006, **8**, 1357–1370.
12 T. Rimza, S. Saha, C. Dhand, N. Dwivedi, S. S. Patel, S. Singh and P. Kumar, *ChemSusChem*, 2022, **15**, e202200281.
13 M. Mohan, V. K. Sharma, E. A. Kumar and V. Gayathri, *Energy Storage*, 2019, **1**, e35.
14 X. Wu, Y. Chen, Z. Xing, C. W. K. Lam, S.-S. Pang, W. Zhang and Z. Ju, *Adv. Energy Mater.*, 2019, **9**, 1900343.
15 M. Hu, H. Zhang, T. Hu, B. Fan, X. Wang and Z. Li, *Chem. Soc. Rev.*, 2020, **49**, 6666–6693.
16 P. Kumar, S. Singh, S. Hashmi and K.-H. Kim, *Nano Energy*, 2021, **85**, 105989.
17 D. Farrusseng, S. Aguado and C. Pinel, *Angew. Chem., Int. Ed.*, 2009, **48**, 7502–7513.
18 L. Zhu, X.-Q. Liu, H.-L. Jiang and L.-B. Sun, *Chem. Rev.*, 2017, **117**, 8129–8176.
19 S. Ma and H.-C. Zhou, *Chem. Commun.*, 2010, **46**, 44–53.
20 S.-Y. Ding and W. Wang, *Chem. Soc. Rev.*, 2013, **42**, 548–568.
21 J. Wang and S. Zhuang, *Coord. Chem. Rev.*, 2019, **400**, 213046.
22 X. Zhao, P. Pachfule and A. Thomas, *Chem. Soc. Rev.*, 2021, **50**, 6871–6913.
23 H. Jiang, W. Shyy, M. Liu, L. Wei, M. Wu and T. Zhao, *J. Mater. Chem. A*, 2017, **5**, 672–679.
24 N. Khossossi, Y. Benhouria, S. R. Naqvi, P. K. Panda, I. Essaoudi, A. Ainane and R. Ahuja, *Sustainable Energy Fuels*, 2020, **4**, 4538–4546.
25 T. Zhang, Y. Ma, B. Huang and Y. Dai, *ACS Appl. Mater. Interfaces*, 2019, **11**, 6104–6110.
26 A. Kara, H. Enriquez, A. P. Seitsonen, L. L. Y. Voon, S. Vizzini, B. Aufray and H. Oughaddou, *Surf. Sci. Rep.*, 2012, **67**, 1–18.
27 V. Eswaraiah, Q. Zeng, Y. Long and Z. Liu, *Small*, 2016, **12**, 3480–3502.
28 Y. Yong, H. Cui, Q. Zhou, X. Su, Y. Kuang and X. Li, *Appl. Surf. Sci.*, 2019, **487**, 488–495.
29 Y. Z. Abdullahi, F. Ersan, Z. D. Vatansever, E. Aktürk and O. Ü. Aktürk, *J. Appl. Phys.*, 2020, **128**, 113903.
30 T. Li, C. He and W. Zhang, *J. Mater. Chem. A*, 2019, **7**, 4134–4144.
31 Y. Z. Abdullahi, A. Tigli and F. Ersan, *Phys. Rev. Appl.*, 2023, **19**, 014019.
32 R. Raccichini, A. Varzi, S. Passerini and B. Scrosati, *Nat. Mater.*, 2015, **14**, 271–279.
33 P. A. Denis and F. Iribarne, *Comput. Theor. Chem.*, 2015, **1062**, 30–35.
34 V. Mahamiya, A. Shukla and B. Chakraborty, *Int. J. Hydrogen Energy*, 2022, **47**, 41833–41847.
35 T. Kaewmaraya, N. Thatsami, P. Tangpakonsab, R. Kinkla, K. Kotmool, C. Menendez, K. Aguey-Zinsou and T. Hussain, *Appl. Surf. Sci.*, 2023, **629**, 157391.
36 T. Hussain, M. Hankel and D. J. Searles, *J. Phys. Chem. C*, 2017, **121**, 14393–14400.
37 N. F. Martins, A. S. Maia, J. A. Laranjeira, G. S. Fabris, A. R. Albuquerque and J. R. Sambrano, *Int. J. Hydrogen Energy*, 2024, **51**, 98–107.
38 X. Zhang, F. Chen, B. Jia, Z. Guo, J. Hao, S. Gao, G. Wu, L. Gao and P. Lu, *Int. J. Hydrogen Energy*, 2023, **48**, 17216–17229.
39 I. Djebablia, Y. Z. Abdullahi, K. Zanat and F. Ersan, *Int. J. Hydrogen Energy*, 2024, **66**, 33–39.
40 L.-J. Ma, Y. Sun, J. Jia and H.-S. Wu, *Fuel*, 2024, **357**, 129652.
41 Y. Fu, J. Xiang, Y. Xie, X. Gong, Y. Xu, Q. Zhao, Y. Liu, J. Xu and W. Liu, *Comput. Mater. Sci.*, 2024, **238**, 112951.
42 X. Gong, Y. Fu, Y. Xu, W. Liu and J. Xu, *Mater. Today Commun.*, 2024, **40**, 109626.
43 Y. Xie, L. Chen, J. Xu and W. Liu, *RSC Adv.*, 2022, **12**, 20088–20095.
44 Y. Xu, Y. Fu, X. Gong, J. Xu and W. Liu, *Mater. Today Commun.*, 2024, **41**, 110394.
45 P. Panigrahi, A. Kumar, A. Karton, R. Ahuja and T. Hussain, *Int. J. Hydrogen Energy*, 2020, **45**, 3035–3045.
46 P. Panigrahi, M. Desai, M. K. Talari, H. Bae, H. Lee, R. Ahuja and T. Hussain, *Int. J. Hydrogen Energy*, 2021, **46**, 7371–7380.
47 J. I. Jason, Y. Pal, P. Anees, H. Lee, T. Kaewmaraya, T. Hussain and P. Panigrahi, *Int. J. Hydrogen Energy*, 2024, **50**, 455–463.
48 M. Singh, A. Shukla and B. Chakraborty, *Sustainable Energy Fuels*, 2023, **7**, 996–1010.
49 K. Boezar, A. Reisi-Vanani and M. Dehkhodaei, *Int. J. Hydrogen Energy*, 2021, **46**, 38370–38380.
50 P. Hohenberg and W. Kohn, *Phys. Rev.*, 1964, **136**, B864.
51 G. Kresse and J. Furthmüller, *Phys. Rev. B: Condens. Matter Mater. Phys.*, 1996, **54**, 11169.
52 J. P. Perdew, K. Burke and M. Ernzerhof, *Phys. Rev. Lett.*, 1996, **77**, 3865.
53 S. Grimme, J. Antony, S. Ehrlich and H. Krieg, *J. Chem. Phys.*, 2010, **132**, 154104.
54 D. Nazarian, P. Ganesh and D. S. Sholl, *J. Mater. Chem. A*, 2015, **3**, 22432–22440.
55 H. J. Monkhorst and J. D. Pack, *Phys. Rev. B: Solid State*, 1976, **13**, 5188.
56 G. J. Martyna, M. L. Klein and M. Tuckerman, *J. Chem. Phys.*, 1992, **97**, 2635–2643.
57 R. F. Bader, *Acc. Chem. Res.*, 1985, **18**, 9–15.
58 K. Momma and F. Izumi, *J. Appl. Crystallogr.*, 2011, **44**, 1272–1276.
59 E. Durgun, S. Ciraci and T. Yildirim, *Phys. Rev. B: Condens. Matter Mater. Phys.*, 2008, **77**, 085405.
60 Y. Z. Abdullahi and F. Ersan, *Comput. Mater. Sci.*, 2024, **242**, 113103.
61 K. Alhameedi, T. Hussain, H. Bae, D. Jayatilaka, H. Lee and A. Karton, *Carbon*, 2019, **152**, 344–353.
62 A. Hashmi, M. U. Farooq, I. Khan, J. Son and J. Hong, *J. Mater. Chem. A*, 2017, **5**, 2821–2828.

63 A. M. Satawara, G. A. Shaikh, S. K. Gupta, A. N. Andriotis, M. Menon and P. Gajjar, *Int. J. Hydrogen Energy*, 2023, **48**, 25438–25449.
64 C. Kittel and P. McEuen, *Introduction to Solid State Physics*, John Wiley & Sons, 2018.
65 W. Othman, W. Alfalasi, T. Hussain and N. Tit, *J. Energy Storage*, 2024, **98**, 113014.
66 Y. Gong, D. Chen, B. Guo, S. Chen, Z. Zhu and M. Cheng, *Int. J. Hydrogen Energy*, 2024, **82**, 384–397.
67 S. Nachimuthu, P.-J. Lai, E. G. Leggesse and J.-C. Jiang, *Sci. Rep.*, 2015, **5**, 16797.
68 S. R. Naqvi, T. Hussain, P. Panigrahi, W. Luo and R. Ahuja, *RSC Adv.*, 2017, **7**, 8598–8605.
69 L. Yuan, L. Kang, Y. Chen, D. Wang, J. Gong, C. Wang, M. Zhang and X. Wu, *Appl. Surf. Sci.*, 2018, **434**, 843–849.
70 A. Yadav, B. Chakraborty, A. Gangan, N. Patel, M. Press and L. M. Ramaniah, *J. Phys. Chem. C*, 2017, **121**, 16721–16730.